agronomy

Article

Construction and Test of Baler Feed Rate Detection Model Based on Power Monitoring

Huaiyu Liu [1,†], Ning Gao [1,†], Zhijun Meng [2], Anqi Zhang [1,*], Changkai Wen [1], Hanqing Li [1] and Jing Zhang [3]

1 Research Center of Intelligent Equipment, Beijing Academy of Agriculture and Forestry Sciences, Beijing 100097, China
2 Information Technology Research Center, Beijing Academy of Agriculture and Forestry Sciences, Beijing 100097, China
3 AgChip Science and Technology (Beijing) Co., Ltd., Beijing 100097, China
* Correspondence: zhangaq@nercita.org.cn
† These authors contributed equally to this work.

Abstract: The existing methods of measuring the baler feed rate seldom consider the influence of machine vibration on the sensor signal during field operation, which leads to the low detection accuracy and poor stability of feeding quantity detection. We established a feed rate detection model of a baler based on power monitoring of the pickup platform. Through the dynamic analysis of the pickup platform, the functional relationship between the working power of the pickup platform and the feed rate was constructed. A power monitoring system of the pickup platform was developed, and the model construction experiment of the working power and the feed rate was performed. The influence mechanism of different running speeds on the torque noise signal of the power input shaft of the pickup platform was explored. The frequency of the noise signal was mainly concentrated at 0.5–6 Hz and 9–13 Hz employing a fast Fourier transform, and the noise signal was eliminated by the frequency-domain-filtering method. The function model of working power and feed rate of the pickup platform was established based on signal processing, and the determination coefficient R^2 of the model was 0.9796. The field experiment results show that when the feed rate of the baler is between 1.6 and 4.88 kg/s, the determination coefficient R^2 and $RMSE$ between the actual and predicted feed rate are 0.989 and 0.2, respectively. The relative error range of feed-rate prediction is −9.37–8.77%, which indicates that the model has high detection accuracy and good stability and meets the requirements of feed-rate monitoring of a baler in field operation.

Keywords: baler; feed rate; pickup platform; working power; frequency domain filtering; model

check for updates

Citation: Liu, H.; Gao, N.; Meng, Z.; Zhang, A.; Wen, C.; Li, H.; Zhang, J. Construction and Test of Baler Feed Rate Detection Model Based on Power Monitoring. *Agronomy* **2023**, *13*, 425. https://doi.org/10.3390/agronomy13020425

Academic Editor: William David Batchelor

Received: 17 December 2022
Revised: 19 January 2023
Accepted: 28 January 2023
Published: 31 January 2023

1. Introduction

Straw is a crucial biomass resource in agricultural production. The recycling of straw can not only promote the development of comprehensive straw utilization technology but also effectively improve the ecological environment [1–6]. To improve the collection efficiency of crop straw and reduce the transportation cost, balers were usually used to pick up the scattered straw in the field and press it into a high-density bundle structure [7,8]. The baler's feed rate is the critical index to evaluate the baler's functional performance and working state. If the feed rate is too low, the operation efficiency of the baler will be affected, and the operation cost will be increased. An excessive feeding amount will quickly lead to a blockage of the pickup platform, which will lead to operation failure of the transmission mechanism of the baler and seriously reduce the operation efficiency [9,10]. Therefore, obtaining the baler's feed rate in real time and keeping it in the best state can not only guide the driver to complete the straw-bundling operation efficiently but also have important practical significance for indirectly improving the comprehensive utilization rate of regional straw and improving the ecological environment.

Currently, the methods of crop feed-rate detection can be divided into extrusion force measurement, oil pressure measurement, image recognition, and torque and power measurement methods according to the principle [11–16]. Jie Zhan researched the relationship between feed rate, extrusion force and sensor signal based on the principle of extrusion pressure measurement [17]. Gomez-Gil developed a mathematical model of the grain-combine feed rate and running speed using GPS technology and particle weight sensors [18]. Sun Yifan developed a mathematical model of power-input-shaft torque, height, grain moisture content and feed rate of a combine harvester pickup platform based on the PSO-BP algorithm [19]. Wang Wei predicted the straw feed rate by monitoring the power of the screw conveyor and established a feeding amount detection model according to the grey theory [9]. Li Ping collected the pressure value of the header lifting cylinder and fitted the feed rate and pressure sensor signal by the least square method [20]. Liu Zhongpeng used an image segmentation algorithm to separate the wheat from the background and obtained the transformation relationship between the feed rate and image pixels by data fitting [15]. To sum up, limited by the working principle and mechanical structure of the baler's pickup platform, the feed-rate detection method based on extrusion force, oil pressure measurement and the image recognition principle was not suitable for the baler. Torque can better reflect the change in feeding amount. However, it is easily affected by uncontrollable variables, such as the angle of the pick-up mechanism in the detection process. As a linear quantity, power has fewer uncontrollable variables that affect its detection accuracy, which can more effectively reflect the change in machine feeding quantity [21]. In addition, the related research seldom considers the influence of machine vibration on sensor signals in actual operation, so it is not easy to ensure detection performance in a complex working environment.

Therefore, this study takes the square baler as the research object. Through an analysis of the dynamics of the pickup platform, the functional relationship between the working power of the pickup platform and the feed rate was established. A pick-up platform working power-monitoring system was built to obtain the original torque signal, and frequency domain analysis and filtering were performed. The specific function model of working power and feed rate of the pickup platform was obtained based on signal analysis and processing. Finally, field experiments tested the accuracy and stability of the feed-rate detection model. This study can provide a theoretical reference for the research of online detection technology of baler feed rate.

2. Materials and Methods

2.1. Dynamics Analysis of Pickup Platform

As shown in Figure 1, the overall structure of the pickup platform of the square baler is mainly composed of a power input shaft, picker shaft, pickup elastic teeth, screw conveyor and its shaft, which mainly completes the functions of straw pickup and centralizes backwards conveying. The working power of the pickup platform comes from the power input shaft. The power is transferred to the screw conveyor through the belt and drives the screw conveyor to rotate and then the power is transferred to the picker shaft through the chain. During continuous rotation, the picker shaft drives the elastic teeth to throw the ground straw to the screw conveyor. The screw conveyor squeezes the straw to the feeding mechanism during continuous rotation to complete the pick-up operation. According to the pitch diameter of the pulley and the transmission mode of each shaft, the transmission ratio among the power input shaft, screw conveyor shaft, and picker shaft is 1. Through the analysis of the operational characteristics of the pickup platform, it can be seen that the rotational speed of each shaft is consistent when the pickup platform works.

The power input shaft provides the working power for the square baler pickup platform, and the power input shaft power is the pickup platform power when the square baler is working. From the mathematical relationship of power, torque, and rotational speed, the total power of the pickup platform when the power input shaft is working is

$$P = Tn/9550 \tag{1}$$

where P is the total power of the power input shaft in kW; T is the total torque of the power input shaft in N·m; n is the rotational speed of each shaft of the pickup platform in r/min.

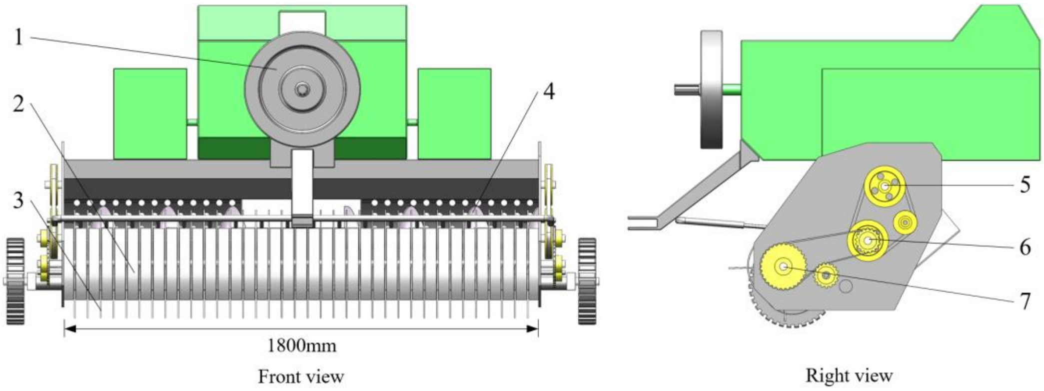

Figure 1. Structure diagram of square baler pickup platform: (**1**) flywheel; (**2**) pickup elastic teeth; (**3**) pickup plate; (**4**) screw conveyor; (**5**) power input shaft; (**6**) screw conveyor shaft; (**7**) picker shaft.

The pickup platform mainly consisted of a picker and a screw conveyor. According to the energy conservation theorem, the total power of the pickup platform can be decomposed into

$$P = P_0 + P_i + P_j \tag{2}$$

where P_0 is the total loss power of the transmission mechanism in kW, P_i is the total power of pickup in kW, and P_j is the total power of screw conveyor in kW.

(1) Torque analysis of picker shaft

The total torque T_i of the picker shaft can be decomposed into no-load torque T_{i1} and working torque T_{i2}, in which the no-load torque is related to its gravity. The working torque is mainly due to the torque produced by the gravity of the straw. Because the length of the elastic teeth extending out of the retaining ring is short, it can be considered that the straw is approximately concentrated at the end of the elastic teeth of the pickup, and thus

$$\begin{cases} T_{i1} = m_i g R \\ T_{i2} = \rho L h v_0 g R \end{cases} \tag{3}$$

$$q = \rho L h v_0 \tag{4}$$

$$T_i = (m_i + q) g R \tag{5}$$

where m_i is the weight of the picker in kg, ρ is the natural laying density of straw in kg/m^3, L is the pickup width in m, h is the natural laying thickness of straw in m, v_0 is the running speed of the baler in m/s, g is the acceleration of gravity in m/s^2, R is the radius of gyration of pickup elastic teeth in m, and q is the theoretical feed rate of straw in kg/s.

(2) Torque analysis of screw conveyor shaft

The total torque T_j of the screw conveyor shaft can be decomposed into no-load torque T_{j1} and working torque T_{j2}, and the no-load torque is related to its gravity. The working torque is mainly caused by the extrusion force F_r perpendicular to the surface of the spiral blade and the tangential friction resistance F_f along the spiral blade under the action of extrusion and the conveying of the straw by the spiral conveyor, which is not only affected by the extrusion force F_r perpendicular to the surface of the spiral blade. The friction resistance F_f is proportional to the extrusion force F_r of straw on spiral leaves. Assuming that the friction coefficient between the straw and screw conveyor is f, then

$$\begin{cases} T_{j1} = D(m_j g - F_r) \\ T_{j2} = Dqg + DF_f \end{cases} \tag{6}$$

$$F_f = f \cdot F_r \tag{7}$$

where D is the radius of gyration of the picker elastic teeth in m and m_j is the weight of the screw conveyor in kg.

According to [22–24], the extrusion force F_r is related to the degree of straw extrusion, and thus

$$F_r = K_p \cdot (\frac{C_{max}}{\delta})^N \tag{8}$$

$$C_{max} = \frac{q\lambda}{[(1+\lambda)\rho V_s w]} \tag{9}$$

where K_p is the coefficient, C_{max} is the natural laying thickness of non-grain materials in mm, δ is the clearance between spiral blade and intaglio in mm, N is a real number, λ is the mass ratio of fruit and seedlings, V_s is the average linear velocity of straw in screw conveyor in m/s, and w is the width of the screw conveyor in m.

In this study, the experimental object is crop straw, and λ approximates it to infinity; thus, Formula (9) can be simplified as

$$C_{max} = \frac{q}{\rho V_s w} \tag{10}$$

From Equations (6)–(10), it can be seen that the total torque of the screw conveyor shaft is

$$T_j = Dqg + D[m_j g + K_p(\frac{1}{\rho V_s w \delta})^N q^N (f-1)] \tag{11}$$

From Equations (2), (5), and (11), it can be seen that the total torque T of the power input shaft of the pickup platform is

$$T = T_0 + (m_i + q)gR + Dqg + D[m_j g + K_p(\frac{1}{\rho V_s w \delta})^N q^N (f-1)] \tag{12}$$

(3) Power analysis of pickup platform

After excluding the torque caused by the gravity of the picker and screw conveyor, the working torque T' of the pickup platform is

$$T' = T_0 + qg(R+D) + DfK_p(\frac{1}{\rho V_s w \delta})^N q^N \tag{13}$$

From Equations (1) and (13), it can be seen that the working power T' of the pickup platform is

$$P' = \frac{1}{9550} T_0 n + \frac{1}{9550}(R+D)gnq + \frac{1}{9550} DfnK_p(\frac{1}{\rho V_s w \delta})^N q^N \tag{14}$$

It can be seen from the above formula that when other parameters are constant, and the baler is fed stably and evenly, the working power of the pickup platform is linearly related to the feed rate. The above formula can be simplified to

$$P' = K_0 + K_1 q + K_2 q^N \tag{15}$$

where K_0, K_1, and K_2 are all constant coefficients.

2.2. Field Test Method

2.2.1. Test Equipment and Materials

To explore the specific function model between the working power of the pickup platform and the feed rate, the power-monitoring system of the pickup platform was built, and the system structure is shown in Figure 2. The system consists of a sensor unit and a data-management unit. The sensor unit converts the torque and rotational speed signals of the power input shaft of the pickup platform into voltage signals and pulse signals, respectively. The built-in module of the acquisition instrument converts the two signals into torque and rotational speed data. Following this, it is transmitted to the vehicle data-management unit for display and storage through the RS485 bus. Finally, the power data of the pickup platform are calculated according to Equation (1).

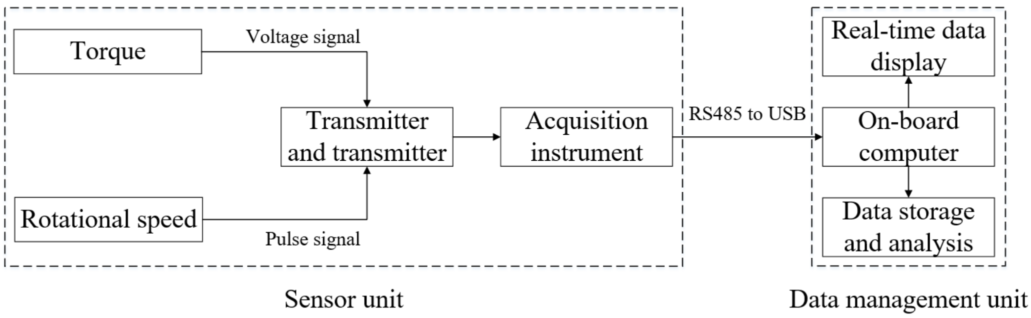

Figure 2. Structural block diagram of a monitoring system.

A DYN-200 torque and rotational speed sensor (Bengbu Dayang Sensing System Engineering Co., Ltd., Bengbu, China) is the test sensor. The torque and rotational speed data of the power input shaft of the pickup platform are collected synchronously through the supporting data management software. Its main parameters are as follows (Table 1):

Table 1. Main parameters of the sensor.

Parameters	Value
Range of torque	±500 N·M
Range of rotational speed	10,000 RPM
Error of measurement	<0.1%
Voltage	DC24 V

To accurately collect the torque and rotational speed data of the power input shaft, a separate power input shaft was designed. The sensor was installed between the power end and the load end of the power input shaft by two couplings and fixed on the rear protective plate of the pickup platform by an installation bracket. The installation diagram is shown in Figure 3.

In October 2022, the model construction test was conducted in the Xiaotangshan National Experiment Station for Precision Agriculture, Changping District, Beijing. The test equipment and materials are shown in Figure 4. Dry wheat straw is the test object. The torque and rotational speed sensor was installed on the power input shaft of the pickup platform of the 9YFQ-2.2 baler (Tianjin Xuanhe Agricultural Machinery Manufacturing Co., Ltd., Tianjin, China). The Lovol Oubao M800-D tractor (Weichai Lovol Heavy Industry Co., Ltd., Weifang, China) pulls the baler and provides operating power. In order to ensure the picking quality of the baler, AMG-300 tractor automatic driving navigation (AgChip Science and Technology (Beijing) Co., Ltd., Beijing, China) was adopted to control the tractor to drive automatically according to the planned path. In addition, other test materials include signs, stopwatches, tape measures, and electronic scales, which were used to divide the test site and accurately measure the working time of the baler.

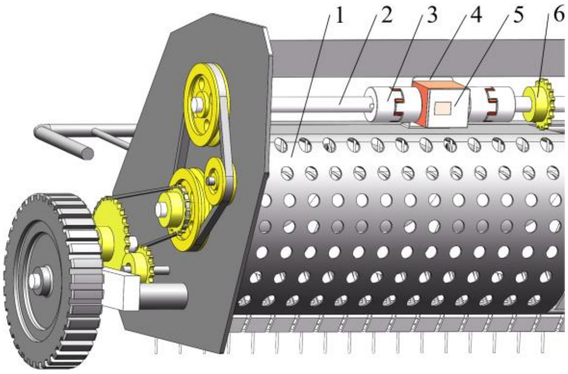

Figure 3. Sensor installation diagram: (**1**) rear protective plate of the pickup platform; (**2**) separate power input shaft; (**3**) coupling; (**4**) installation bracket; (**5**) torque and rotational speed sensor; (**6**) transmission gear.

Figure 4. Test equipment.

2.2.2. Test Methods

In this study, the torque and rotational speed sensors were used to measure the baler's power input shaft's torque and rotational speed data at different running speeds under the field test conditions, and the working time and feed rate of the baler were obtained by manual measurement. To obtain sufficient experimental data and reduce the experimental cost, the size of the field experiment plot was determined to be 20×1.8 m. According to the actual yield and economic coefficient [25–28] of wheat in this experimental field, it can be calculated that 1.5 kg straw should be laid on each square meter of land. In order to ensure the uniform laying of straw, a plot with a length of 20 m was divided into ten sections. The straw was manually weighed and 5.4 kg straw was laid at each interval. The test site is shown in Figure 5.

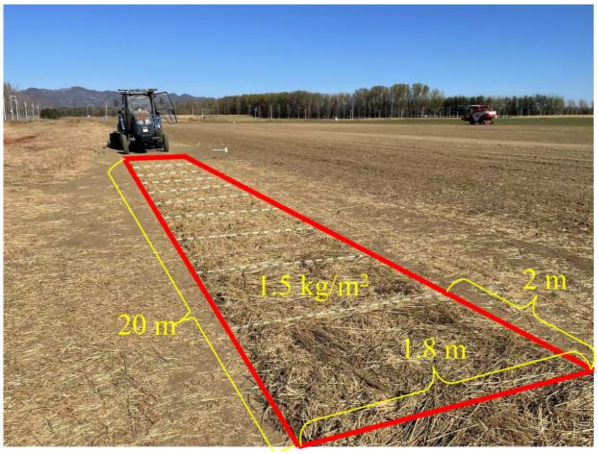

Figure 5. Test site.

Considering the influence of ground height on sensor data acquisition, this study determined through many no-load tests that the appropriate height for picking up elastic teeth from the ground of the baler is 50 mm. Before each test, the pickup elastic teeth were adjusted to the appropriate height, and the sensor was cleared. The tester used a stopwatch to measure the working time of the baler and inserted signs at the starting and ending positions of the test plot. The tester starts timing at the moment when the pickup platform of the baler touches the start sign and stops timing at the moment when the pickup platform touches the end sign. During data acquisition, a vehicle-mounted data-management software is used to measure the torque and rotational speed of the baler's power input shaft under no-load and load conditions. The difference between the average torque of the power input shaft under load and the average torque under no load is taken as the working torque of this test, and the rotational speed is the average value of the rotational speed data under load.

$$Q = \frac{M}{t} \tag{16}$$

where Q is the actual feed rate of the baler in kg/s, M is the total amount of straw harvested in kg, and t is the operation time in s.

2.3. Signal Processing Method

In the process of sensor signal acquisition, the vibration caused by the mechanical transmission of the baler and ground bumping greatly influences the sensor signal's stability [29]. In this study, the frequency domain information of the original torque signal of the power input shaft was obtained by Fourier transform, the concentrated frequency band of the noise signal was found, and the torque noise signal was eliminated by frequency domain filtering.

A discrete Fourier transform is a discrete form of Fourier transform in the time domain and frequency domain, which is the sampling of the Fourier transform of time domain signal in discrete time [30–32]. The main idea is to establish the function-mapping relationship between the signal's frequency spectrum with time as the independent variable and frequency as the dependent variable from the finite points of the Fourier transform in an ordered long sequence. The continuous Fourier transform formula of an analogue signal $x(t)$ is as follows

$$X(w) = \int_{-\infty}^{\infty} x(t)e^{-jwt}dt \tag{17}$$

$x(t)$ becomes $X(nT)$ after T sampling periods. If $X(nT)$ is an B point finite-length sequence, then DFT is:

$$X(k) = DFT[x(n)] = \sum_{n=0}^{N-1} x(n)W_N^{nk} = \sum_{n=0}^{N-1} x(n)e^{-j\frac{2\pi}{N}nk}, k = 0, 1, \cdots, B-1 \tag{18}$$

Because the computational complexity of the DFT algorithm increases with the increase in ordered length signal, it does not meet the needs of practical engineering applications. The FFT algorithm transforms a long DFT operation into several short DFT operations employing periodicity $W_N^{nk} = W_N^{(n+N)k}$, symmetry $W_N^{n+N/2} = -W_N^n$, and reducibility $W_N^{nk} = W_{mN}^{mnk}$ of the DFT algorithm.

3. Results and Discussion

3.1. Signal Analysis and Processing Results

In this study, the test results of a baler working at 5.57 km/h are taken as an example. The time domain diagram of its original torque and rotational speed signal is shown in Figure 6. As seen from the figure, when the baler works, the mechanical vibration and ground turbulence significantly impact the torque sensor signal. The data variability and overall smoothness were poor. The rotational speed signal was relatively stable, and the overall distribution was about 278 r/min. The standard deviation was 6.18 r/min. In this study, we will analyze the causes of torque signal noise.

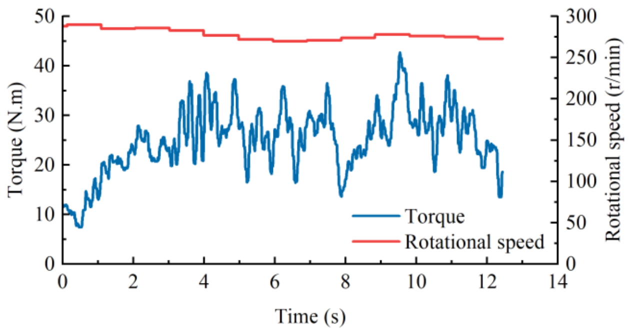

Figure 6. Time domain diagram of original torque and rotational speed signal.

The frequency domain information of torque signal under different running speeds was obtained by fast Fourier transform to explore the influence mechanism of running speed on the torque noise signal. Figure 7 is a spectrum diagram of the torque signal of the baler in the static and working state under different running speeds. As seen from Figure 7, under different running speeds, the amplitude of the torque noise signal when the baler works is more prominent than when it is at rest. With the baler's increased running speed, the noise signal's amplitude when the machine works gradually increases. The reason is that when the baler is running at a low speed, the vibration of the machine produced by the power system is the primary source of the noise signal, and the amplitude of the noise signal in the two states is equivalent. With the increased running speed of the baler, the bump caused by ground fluctuation becomes the primary source of the noise signal, and the amplitude of the noise signal increases with the increase in running speed.

As shown in Figure 7, the torque noise signals were mainly concentrated at 0.5–6 Hz and 9–13 Hz. In this study, the noise reduction of the original torque signal was conducted by the frequency-domain-filtering method. The torque signal collected by the baler at the running speed of 5.57 km/h was taken as the object. Figure 8 is a time domain diagram of working torque signals before and after processing. After filtering, the variability of torque data was reduced, and the overall smoothness of the data was improved. Data fluctuation was due to the change in torque caused by an uneven straw feed rate during baler operation.

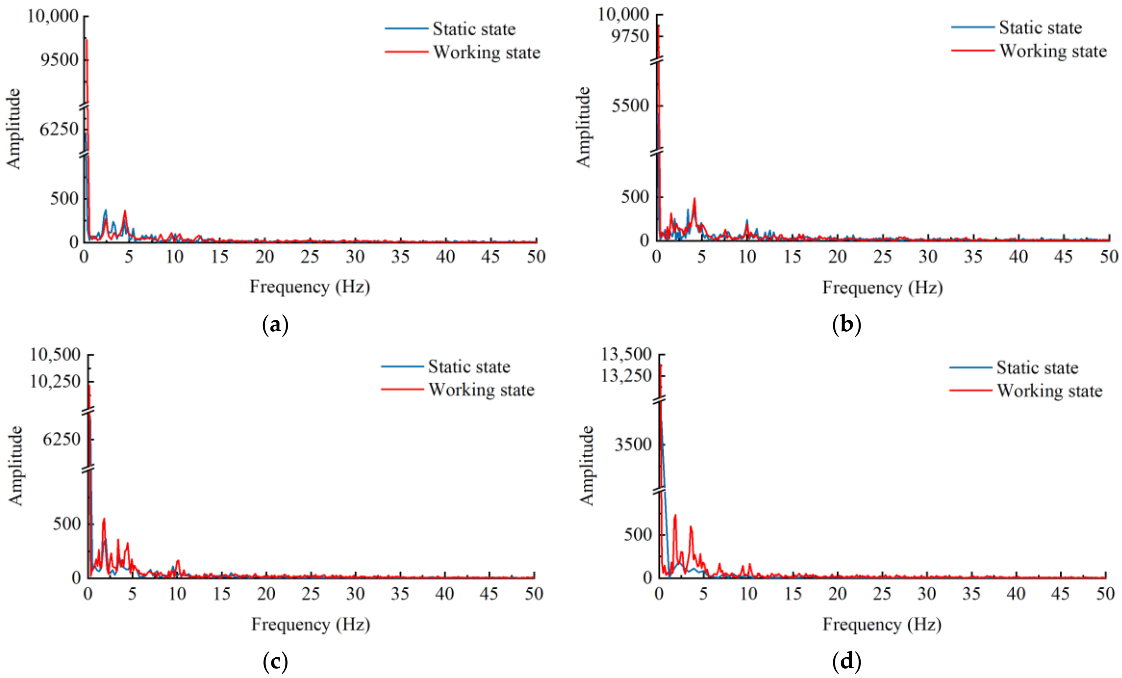

Figure 7. Spectrum diagram of torque signal at different running speeds: (**a**) 3.17 km/h; (**b**) 4.14 km/h; (**c**) 5.57 km/h; (**d**) 7.13 km/h.

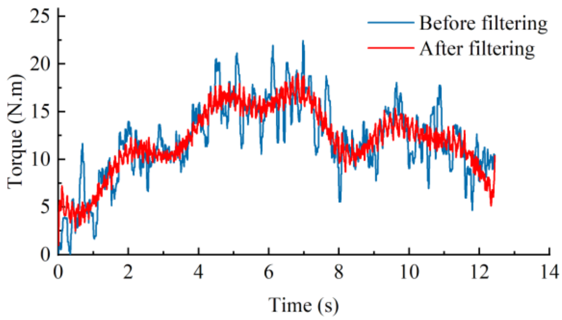

Figure 8. Time domain diagram before and after signal processing.

3.2. Construction Results of Feed-Rate Detection Model

In this study, we used the frequency-domain-filtering method to process all the original torque data in the above tests. According to Equation (1), the average working power of the pickup platform for each group of tests was calculated, and the test results are shown in Table 2.

In this study, the multivariate linear regression method was used to establish a specific functional model of working power and feed rate, and the performance of the model was evaluated by R^2 (efficient of determination) and *RMSE* (root mean square error). R^2 was used to evaluate the correlation degree between the actual value and the predicted value of the feed rate. The closer R^2 is to 1, the better the correlation degree between the actual value and the predicted value of the feed rate. *RMSE* was used to evaluate the prediction ability of the model. A smaller *RMSE* indicates a better generalization ability of the model.

In this study, the relationship curve between the working power of the pickup platform and the feed rate fitted by SPSS26 is shown in Figure 9.

Table 2. Test results.

Test	Running Speed (km/h)	Harvest (kg)	Working Torque (N·m)	Rotational Speed (r/min)	Working Power (kW)	Feed Rate (kg/s)
1	3.17	30.4	6.23	292.7	0.1909	1.34
2	4.24	32.28	8.66	393.3	0.3566	1.90
3	7.13	20.29	7.23	375	0.2839	2.01
4	5.57	30.61	11.97	345.8	0.4334	2.37
5	6.46	28.57	12.05	342.1	0.4317	2.56
6	5.78	32.81	15.6	365.5	0.5970	2.64
7	7.07	31.06	16.85	338.9	0.5980	3.05
8	8.41	29.63	17.95	391	0.7349	3.46
9	9.35	30.18	26.77	347.4	0.9738	3.92
10	10.64	32.02	33.79	384.3	1.3597	4.73
11	10.53	32.93	29.05	386.2	1.1748	4.81
12	10.48	36.13	40.38	379.9	1.6063	5.26

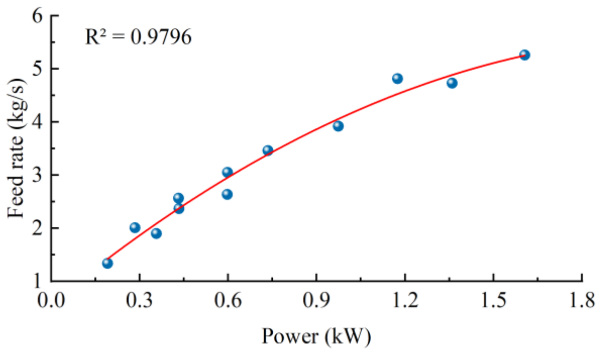

Figure 9. Fitting results of working power and feed rate.

As seen from Figure 9, the feed rate increases with the increase in power, and there is an excellent linear relationship between them. The determination coefficient R^2 was 0.9796, and the functional relationship between the working power of the pickup platform and the feed rate is shown in Equation (19).

$$Q = -1.0433P'^2 + 4.5791P' + 0.5859 \tag{19}$$

3.3. Field Verification Test Results

In order to verify the accuracy and effectiveness of the model in the field operation of the baler, 11 groups of field verification experiments were conducted according to the above test methods and signal processing methods. The test site is shown in Figure 10.

In the experiment, the running speed of the baler ranged from 4.14 km/h to 10.37 km/h, and the feed rate ranged from 1.62 kg/s to 4.88 kg/s. The feed-rate detection model calculated the predicted value of the feed rate of each group of tests. The relationship between the actual value and the predicted value of the feed rate in each group was compared and analyzed. Figure 11 shows the distribution of actual and predicted values of baler feed rate in each group of tests. According to the test results, the determination coefficient R^2 between the actual value and the predicted value of the baler feed rate is 0.989, the *RMSE* is 0.2, and the relative error range of the feed-rate prediction is −9.37–8.77%. Therefore, the results of field experiments prove that the model has high accuracy and good effectiveness, and meets the needs of monitoring the baler feed rate in the field operation.

Figure 10. Field experiment.

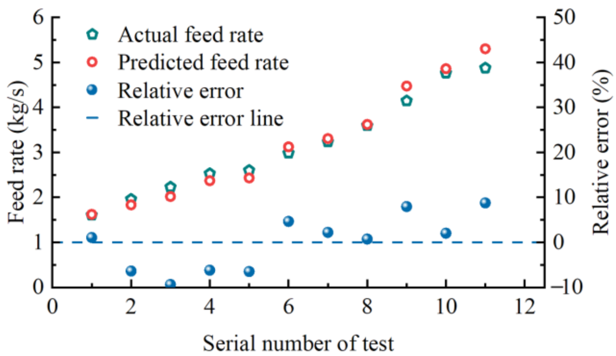

Figure 11. Field test results.

4. Conclusions

The existing methods of measuring the baler feed rate seldom consider the influence of machine vibration on the sensor signal during field operation, which leads to a low detection accuracy and poor stability in feeding-quantity detection. In this study, we established a model for measuring the baler feed rate based on the power monitoring of the pickup platform. We verified the accuracy and effectiveness of the model's predictions through field experiments. The conclusions of this study are as follows:

Through the dynamic analysis of the baler pickup platform, the functional relationship between the working power of the pickup platform and the feed rate was obtained. A power-monitoring system for the baler pickup platform was developed, which realizes the real-time collection of torque and rotational speed data of the power input shaft. The influence mechanism of the baler running speed on the torque noise signal was analyzed, the main frequency distribution range of the torque noise signal was determined, and the torque noise signal was eliminated by the frequency-domain-filtering method. Finally, a mathematical model of the working power and feed rate of the pickup platform was constructed, and a field experiment of model performance verification was performed.

Noise signal analysis results showed that when the sampling frequency of the system was 200 Hz, the frequency of torque noise signal was distributed in the ranges 0.5–6 Hz and 9–13 Hz. The results of the feed-rate detection model construction showed that the R^2 of the model was 0.9796 when the baler feed rate was between 1.34 and 5.26 kg/s. The results of field experiments showed that the R^2 between the actual and predicted values was 0.989, the *RMSE* was 0.2, and the relative error range of model prediction was −9.37–8.77%. The feed-rate detection model has high accuracy and stability.

Currently, we have only established a model to detect the baler feed rate, but the model still needs to be integrated into the feed-rate monitoring device and has yet to be verified in field trials. In future research, we will develop a control system for the pickup operation of the baler based on feed-rate monitoring. The model in this study will be integrated into the control system. The real-time and accurate control of the baler feed rate in field operation may solve the problem that the control object (such as running speed and pickup height) does not match the feed rate due to the poor monitoring effect of the feed rate in the current baler feed-rate control system, which leads to a low operating efficiency of the baler and easy failure of the transmission mechanism. This study can provide a new technical scheme for the research and development of the feeding-monitoring system of the baler.

Author Contributions: Conceptualization, H.L. (Huaiyu Liu) and N.G.; methodology, Z.M. and A.Z.; software, C.W.; validation, H.L. (Hanqing Li); formal analysis, J.Z.; investigation, C.W.; resources, Z.M. and A.Z.; data curation, H.L. (Huaiyu Liu); writing—original draft preparation, H.L. (Huaiyu Liu) and N.G.; writing—review and editing, H.L. (Huaiyu Liu) and N.G.; visualization, H.L. (Huaiyu Liu); supervision, Z.M.; project administration, Z.M.; funding acquisition, A.Z. All authors have read and agreed to the published version of the manuscript.

Funding: This research was funded by the National Key Research and Development Plan of China (Grant No. 2021YFD200050302), the Innovation Capacity Building Project of Beijing Academy of Agriculture and Forestry Sciences (Grant No. KJCX20200416) and Focus on Research and Development Plan of Shandong Province of China (Major Scientific and Technological Innovation Project) (Grant No. 2022CXGC010608).

Data Availability Statement: All data are presented in this article in the form of figures or tables.

Acknowledgments: We would like to thank the “Research Center of Intelligent Equipment, Beijing Academy of Agriculture and Forestry Sciences”, “Information Technology Research Center, Beijing Academy of Agriculture and Forestry Sciences” and “AgChip Science and Technology (Beijing) Co., Ltd.”.

Conflicts of Interest: The authors declare no conflict of interest.

References

1. Li, S.; Ji, X.; Deng, K.; Zhu, J.; Li, C.; Jian, Y.; Peng, H. Analysis of Regional Distribution Patterns and Full Utilization Potential of Crop Straw Resources. *Trans. Chin. Soc. Agric. Eng.* **2020**, *36*, 221–228. [CrossRef]
2. Liu, S.; Li, D.; Huang, J.; Ma, C.; Wang, H.; Yu, Z.; Qu, X.; Zhang, L.; Han, T.; Du, J.; et al. Temporal and Spatial Distribution Characteristics of Rice Stalk Resources and its Potential of Synthetic Fertilizers Substitution Returning to Farmland in China from 1988 to 2018. *Trans. Chin. Soc. Agric. Eng.* **2021**, *37*, 151–161. [CrossRef]
3. Cong, H.; Meng, H.; Yu, J.; Ye, B.; Yao, Z.; Feng, J.; Yu, B.; Qin, C.; Huo, L.; Yuan, Y.; et al. Analysis of Long-term Mechanism for Development of Straw Industry in Northeast China under Guidance of “Green-concept”. *Trans. Chin. Soc. Agric. Eng.* **2021**, *37*, 314–321. [CrossRef]
4. Huo, L.; Yao, Z.; Zhao, L.; Luo, J.; Zhang, P. Contribution and Potential of Comprehensive Utilization of Straw in GHG Emission Reduction and Carbon Sequestration. *Trans. Chin. Soc. Agric. Mach.* **2022**, *53*, 349–359. [CrossRef]
5. Meng, Z.; Liu, H.; An, X.; Yin, Y.; Jin, C.; Zhang, A. Prediction Model of Wheat Straw Moisture Content Based on SPA-SSA-BP. *Trans. Chin. Soc. Agric. Mach.* **2022**, *53*, 231–238, 245. [CrossRef]
6. Liu, C.; He, Z.; Lu, X. Optimization Analysis of Carbon Emission Reduction from Crop Straw Collection and Transportation under the Sustainable Development goals. *Trans. Chin. Soc. Agric. Eng.* **2022**, *38*, 239–248. [CrossRef]
7. Zhang, A.; Meng, Z.; Chen, L.; Wu, G.; Cong, Y.; An, X. Design and Experiment of Dynamic Weighing System for Small Square Baler. *Trans. Chin. Soc. Agric. Mach.* **2020**, *51*, 170–175. [CrossRef]
8. Liu, H.; Meng, Z.; Zhang, A.; Cong, Y.; An, X.; Fu, W.; Wu, G.; Yin, Y.; Jin, C. On-Line Detection Method and Device for Moisture Content Measurement of Bales in a Square Baler. *Agriculture* **2022**, *12*, 1183. [CrossRef]
9. Wang, W.; Gong, Y.; Bai, X.; Tan, R.; Huang, W. Investigation on Operating Speed Regulation System of Mobile Straw Granulator. *Trans. Chin. Soc. Agric. Mach.* **2021**, *52*, 186–195. [CrossRef]
10. Liu, J.; Guo, H.; Lv, Q.; Li, L. Design of Feeding Control System for Self-propelled Round Baler. *J. Chin. Agric. Mech.* **2021**, *42*, 13–18, 25. [CrossRef]
11. Jim, K. Computer control for the combine. *Agric. Eng.* **1983**, *64*, 7–9.
12. Liang, X.; Chen, Z.; Zhang, X.; Wei, L.; Li, W.; Che, Y. Design and Experiment of On-line Monitoring System for Feed Quantity of Combine Harvester. *Trans. Chin. Soc. Agric. Mach.* **2013**, *44* (Suppl. S2), 1–6. [CrossRef]

13. Li, Y.; Wang, J.; Xu, L.; Tang, Z.; Xu, Z.; Wang, K. Design and Experiment on Adjusting Mechanism of Concave Clearance of Combine Harvester Cylinder. *Trans. Chin. Soc. Agric. Mach.* **2018**, *49*, 68–75. [CrossRef]
14. Luo, S.; Jie, Z. Application of Wireless Dada Acquisition and Virtual Instrument Techniques to Measurement of Combine Feed Quantity. *J. Henan Univ. Sci. Technol. Nat. Sci.* **2010**, *31*, 72–75+111–112. [CrossRef]
15. Liu, Z.; Zhao, J.; Liu, L. Study on Wheat Harvester Crop Density Detection During Maturity Based on the Improved Algorithms. *J. Agric. Mech. Res.* **2015**, *37*, 49–52. [CrossRef]
16. John, S.; Michael, P.M.; Gary, W.K. Combine feed rate sensors. *Trans. ASAE* **1985**, *28*, 2–5. [CrossRef]
17. Jie, Z.; Chen, J.; Liu, H. Research on Fuzzy Control of Random Feed Quantity of GPS Combine. *Trans. Chin. Soc. Agric. Mach.* **2006**, *37*, 55–58.
18. Gomez Gil, J.; Lopez Lopez, L.J.; Navas Gracia, L.M. The Spatial Low-pass Filtering as an Alternative to Interpolation Methods in the Generation of Combine Harvester Yield Maps. *Appl. Eng. Agric.* **2011**, *27*, 1087–1097. [CrossRef]
19. Sun, Y.; Liu, R.; Zhang, M.; Li, M.; Zhang, Z.; Li, H. Design of Feed Rate Monitoring System and Estimation Method for Yield Distribution Information on Combine Harvester. In *Computers and Electronics in Agriculture*; Elsevier: Amsterdam, The Netherlands, 2022; Volume 201, p. 107322. [CrossRef]
20. Li, P.; Cui, J.; Feng, W.; Zhang, X.; Zhang, T.; Li, Y. Design and Test of Real-time Monitoring System for Feeding Quantity of Small Combine. *J. Agric. Mech. Res.* **2022**, *44*, 240–246. [CrossRef]
21. Sun, Y.; Liu, R.; Ou, H.; Zhang, Z.; Zhang, M.; Li, H. Analysis and Comparison of Feed Rate Detection Methods of Combine Harvester Based on Power Detection. *Trans. Chin. Soc. Agric. Mach.* **2020**, *51*, 118–123. [CrossRef]
22. Huynh, V.M.; Powell, T.; Siddall, J.N. Threshing and Separating Process-a Mathematical Model. *Trans. ASAE* **1982**, *20*, 65–73. [CrossRef]
23. Lu, W.; Zhang, D. Research on the Power Consumption Model of Threshing Cylinder. *J. Agric. Mech. Res.* **2012**, *34*, 44–47. [CrossRef]
24. Lu, W.; Deng, Z.; Zhang, D.; Gao, H.; You, H. Combine Feed Rate Modeling Research. *J. Agric. Mech. Res.* **2013**, *35*, 129–132. [CrossRef]
25. Yu, Q.; Sun, G. Study on the Change of Crop Straw Resources in China. *Mod. Agric.* **2018**, *09*, 13–15.
26. Wang, X. Spatial and Temporal Distribution of Crop Residue Resource in the East, Central-South, and Southwest Regions of China. Doctoral Dissertation, China Agricultural University, Beijing, China, 2014.
27. Wei, M.; Wang, X.; Xie, G. Field Residue of Field Crops and its Temporal Distribution among Thirty-one Provinces of China. *J. China Agric. Univ.* **2012**, *17*, 32–44.
28. Wang, X.; Xue, S.; Xie, G. Value-taking for Residue factor as a Parameter to Assess the Field Residue of Field Crops. *J. China Agric. Univ.* **2012**, *17*, 1–8.
29. Zhang, A.; Meng, Z.; Chen, L.; Wang, P.; Liu, H.; An, X. Signal Analysis and Processing of Dynamic Weighing System for Small Square Baler. *Trans. Chin. Soc. Agric. Mach.* **2020**, *51* (Suppl. S2), 243–248, 260. [CrossRef]
30. Yu, X. Application of Fast Fourier Transform in Signal Processing. *Inf. Rec. Mater.* **2021**, *22*, 184–186. [CrossRef]
31. Wu, J. Fast Fourier Spectrometer Signal Acquisition Technology Based on ZYNQ. Master's Thesis, University of China Academy of Sciences, Shanghai, China, 2021.
32. Wang, C. Research on Fast Fourier Transform Algorithm Based on Eisenstein. Master's Thesis, University of Science and Technology of China, Hefei, China, 2021.